Article

Cell Reports

α/β-Hydrolase Domain 6 Deletion Induces Adipose Browning and Prevents Obesity and Type 2 Diabetes

Graphical Abstract

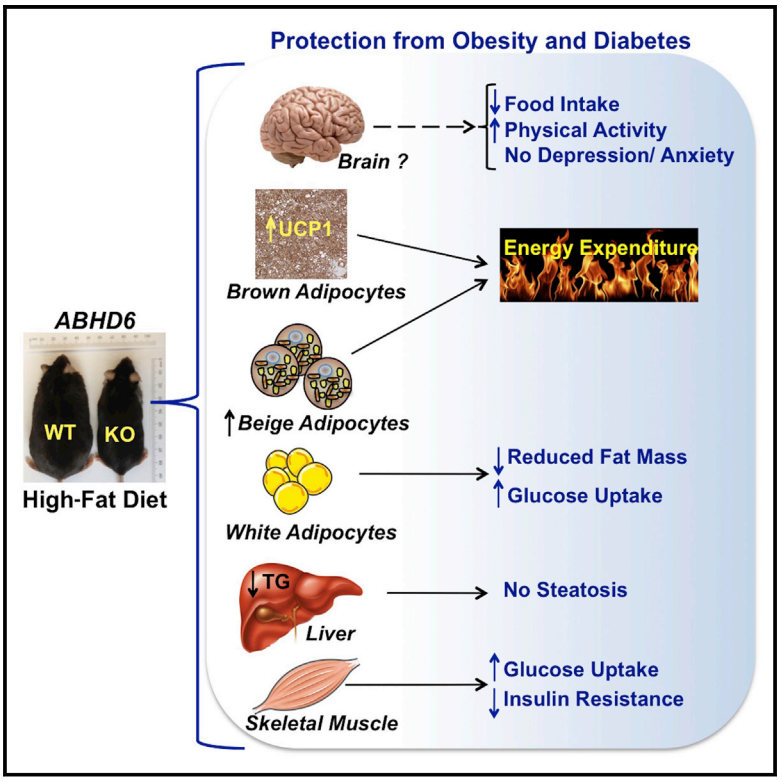

Highlights

- Suppression of the MAG hydrolase ABHD6 protects from diet-induced obesity
- ABHD6-KO enhances energy expenditure and locomotor activity without anxiety
- ABHD6-KO elevates adipose browning and brown adipose function
- Elevated levels of 1-MAG activate PPARα and PPARγ, which enhance adipose browning

Authors

Shangang Zhao, Yves Mugabo, Gwynne Ballentine, ..., J. Mark Brown, S.R. Murthy Madiraju, Marc Prentki

Correspondence

murthy.madiraju@crchum.qc.ca (S.R.M.M.), marc.prentki@umontreal.ca (M.P.)

In Brief

Suppression of ABHD6, a monoacylglycerol hydrolase, was previously shown to promote glucose-stimulated insulin secretion in β cells. Zhao et al. now report that ABHD6 suppression averts diet-induced obesity and enhances adipose browning and brown adipose function via PPARα/γ activation. ABHD6 is a potential therapeutic target for obesity and type 2 diabetes.

Zhao et al., 2016, Cell Reports *14*, 2872–2888
March 29, 2016
http://dx.doi.org/10.1016/j.celrep.2016.02.076

OPEN ACCESS
CellPress

Cell Reports
Article

α/β-Hydrolase Domain 6 Deletion Induces Adipose Browning and Prevents Obesity and Type 2 Diabetes

Shangang Zhao,[1] Yves Mugabo,[1] Gwynne Ballentine,[2] Camille Attane,[1] Jose Iglesias,[1] Pegah Poursharifi,[1] Dongwei Zhang,[1,5] Thuy Anne Nguyen,[1] Heidi Erb,[1] Raphael Prentki,[1] Marie-Line Peyot,[1] Erik Joly,[1] Stephanie Tobin,[1] Stephanie Fulton,[1] J. Mark Brown,[3] S.R. Murthy Madiraju,[1,4,*] and Marc Prentki[1,4,*]

[1]Departments of Nutrition and Biochemistry and Montreal Diabetes Research Center, CRCHUM and Université de Montréal, Montréal, QC H1W 4A4, Canada

[2]Metanome Incorporated, Houston, TX 77046, USA

[3]Department of Cellular and Molecular Medicine, Lerner Research Institute, Cleveland Clinic, Cleveland, OH 44195, USA

[4]Co-senior author

[5]Present address: Diabetes Research Center, Beijing University of Chinese Medicine, Beijing 100029, China

*Correspondence: murthy.madiraju@crchum.qc.ca (S.R.M.M.), marc.prentki@umontreal.ca (M.P.)

http://dx.doi.org/10.1016/j.celrep.2016.02.076

SUMMARY

Suppression of α/β-domain hydrolase-6 (ABHD6), a monoacylglycerol (MAG) hydrolase, promotes glucose-stimulated insulin secretion by pancreatic β cells. We report here that high-fat-diet-fed ABHD6-KO mice show modestly reduced food intake, decreased body weight gain and glycemia, improved glucose tolerance and insulin sensitivity, and enhanced locomotor activity. ABHD6-KO mice also show increased energy expenditure, cold-induced thermogenesis, brown adipose UCP1 expression, fatty acid oxidation, and white adipose browning. Adipose browning and cold-induced thermogenesis are replicated by the ABHD6 inhibitor WWL70 and by antisense oligonucleotides targeting ABHD6. Our evidence suggests that one mechanism by which the lipolysis derived 1-MAG signals intrinsic and cell-autonomous adipose browning is via PPARα and PPARγ activation, and that ABHD6 regulates adipose browning by controlling signal competent 1-MAG levels. Thus, ABHD6 regulates energy homeostasis, brown adipose function, and white adipose browning and is a potential therapeutic target for obesity and type 2 diabetes.

INTRODUCTION

The glycerolipid/free fatty acid cycle, which generates signaling molecules within its lipolysis and lipogenesis segments, plays a role in the regulation of fat storage and mobilization, insulin secretion and action, non-shivering thermogenesis, and energy homeostasis (Nielsen et al., 2014; Prentki and Madiraju, 2008; Zechner et al., 2012). Lipolysis of triglycerides to diacylglycerol, monoacylglycerol (MAG), and glycerol plus fatty acids is catalyzed by the sequential action of adipose triglyceride lipase, hormone sensitive lipase, and MAG lipase (Prentki and Madiraju, 2008; Zechner et al., 2012). Although MAG lipase is thought to be the major MAG hydrolyzing enzyme in many tissues, intracellular breakdown of MAG can also be catalyzed by membrane bound α/β-hydrolase domain 6 (ABHD6) (Blankman et al., 2007). We recently showed ABHD6 as the major MAG hydrolase in pancreatic β cells and that suppression of ABHD6 results in elevated islet 1-MAG levels with enhanced glucose-stimulated insulin secretion through the activation of exocytosis facilitating protein Munc13-1 (Zhao et al., 2014). Whole-body deletion of MAG lipase in mice enhances insulin sensitivity and glucose tolerance without affecting body weight gain or food intake under a high-fat diet (HFD) condition (Taschler et al., 2011). A recent study showed that ABHD6 controls the levels of anti-inflammatory bioactive lipid prostaglandin D2-glycerol ester and that ABHD6 suppression by a pharmacological agent reduces macrophage-mediated inflammation, which contributes to insulin resistance in obesity (Alhouayek et al., 2013). However, the biochemical basis of these beneficial actions and the role of ABHD6 in fuel homeostasis are unknown.

Although obesity is a major contributor to type 2 diabetes (T2D), the current pharmacological approaches for treating obesity and diabetes target different pathways. Several studies showed altered expression of a specific gene, either by knockout or overexpression, to offer protection against diet-induced obesity (DIO), but none of these genes were shown to control both insulin secretion and sensitivity directly (Dirkx et al., 2014; Koh et al., 2013; Liew et al., 2010; Liu et al., 2014; Sumara et al., 2009). It is desirable to identify a metabolic step/pathway that can influence both insulin secretion and action in conjunction with additional beneficial effects on energy homeostasis, such that a single target can be addressed for diabetes and obesity.

Increased energy expenditure via fat oxidation and non-shivering thermogenesis by classical brown adipose tissue (BAT) and by the stimulation of beige adipocytes likely provides an avenue to alleviate the effects of obesity and prevent T2D (Wu et al., 2013). Several recent reports indicate that augmented BAT function and browning of white adipose tissue (WAT)

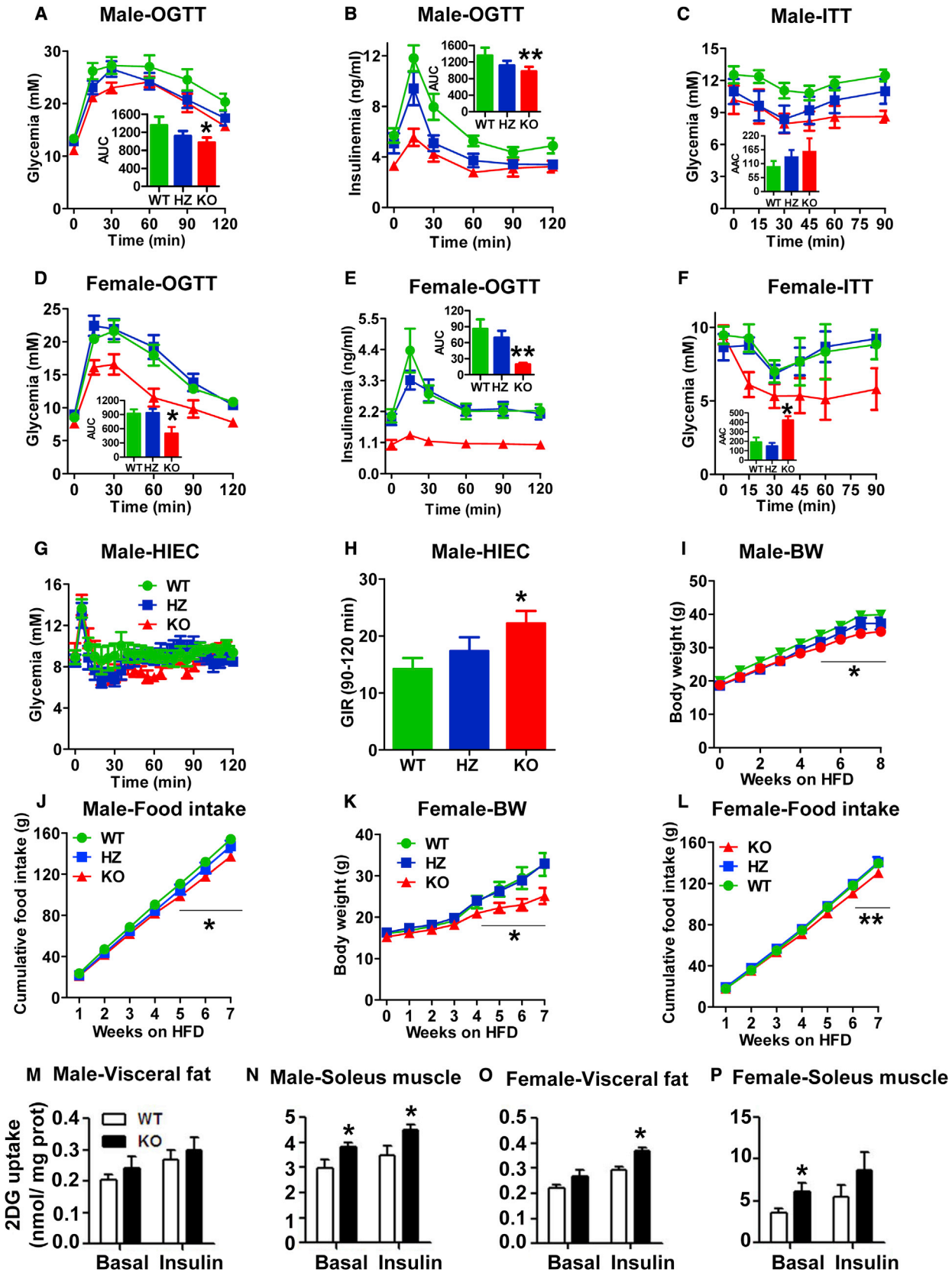

(legend on next page)

enhance glucose tolerance and insulin sensitivity and protect from DIO and obesity-related diabetes (Cereijo et al., 2015; Pfeifer and Hoffmann, 2015; Richard et al., 2010; Rosen and Spiegelman, 2014). Signaling via peroxisomal proliferator-activated receptors (PPAR) is important for beige adipocyte formation (Wu et al., 2012) and the stimulation of BAT (Rosen and Spiegelman, 2014). PPARα plays a role in maintaining brown adipocyte phenotype and in WAT browning (Hondares et al., 2011b; Roberts et al., 2014). Among the endogenous mediators of BAT activation and WAT browning, besides catecholamines, triiodothyronine, FGF21, bone morphogenic proteins (Bartelt and Heeren, 2014), and adenosine (Gnad et al., 2014), certain lipids like prostaglandins and alkyl-ether lipids also play a role by increasing PGC-1α levels or via PPARγ activation (Bartelt and Heeren, 2014). Recent studies suggest that certain lipolytic products may activate PPARs (Badin et al., 2012; Haemmerle et al., 2011; Mottillo et al., 2012) and thus may contribute to adipose browning and BAT activation.

Our earlier study (Zhao et al., 2014) identified a signaling role for MAG and ABHD6 in β cell insulin secretion and glucose homeostasis, but the importance of MAG and ABHD6 in overall energy homeostasis was not addressed. ABHD6 was shown to be induced by high-fat diet in liver but not in BAT (Thomas et al., 2013), indicating this protein to be nutritionally regulated at least in liver. In order to understand the role of ABHD6 and monoacylglycerol in energy homeostasis, we studied whole-body ABHD6-KO mice and DIO mice treated with ABHD6-directed antisense oligo (ASO) or an ABHD6 inhibitor. When fed a HFD, ABHD6-KO mice show a unique phenotype that implicates ABHD6 in obesity, metabolic syndrome, and diabetes. ABHD6-KO mice display a modest reduction of appetite, are protected from obesity, glucose intolerance, insulin resistance, hyperinsulinemia, and hepatic steatosis, and also show enhanced locomotor activity, BAT activity, and WAT browning. The adipose browning effects could be recapitulated by treating wild-type DIO mice with ABHD6 inhibitor or antisense oligonucleotides (ASO) and appear to be, at least in part, intrinsic to adipose tissue involving accumulation of 1-MAG causing PPARα and PPARγ activation.

RESULTS

ABHD6-KO Mice on a High-Fat Diet Show Reduced Weight Gain and Improved Glucose Tolerance and Insulin Sensitivity

Both male and female ABHD6-KO mice fed 60% HFD for 8 weeks showed improved glucose tolerance but much lower insulinemia during OGTT and also enhanced insulin sensitivity during insulin tolerance test (ITT) (Figures 1A–1F). Heterozygous mice showed an intermediate response, more notably for insulinemia. The low insulinemia response in KO mice during OGTT (Figures 1B and 1E) was suggestive of enhanced insulin sensitivity, which was confirmed by ITT (Figures 1C and 1F) and also by hyperinsulinemic-euglycemic clamp (Figures 1G and 1H). Glucose infusion rate (index of insulin sensitivity) in HFD-fed male KO mice was higher as compared to WT mice, with heterozygous mice showing intermediate effect (Figure 1H). During HFD feeding, both male and female ABHD6-KO mice showed less body weight gain (Figures 1I and 1K) and reduced cumulative food intake (Figures 1J and 1L). The decrease in body weight gain was more pronounced in female KO mice (~30% at week 8) as compared to male KO mice (~12% at week 8), whereas the reduction in cumulative food intake (~7% at weeks 6–8) in both sexes was modest, compared to WT mice.

We previously showed that male ABHD6-KO mice on pure C57Bl6/N genetic background when placed on chow diet show normal body weight gain and food intake over a 3- to 24-week period and unaltered insulin sensitivity in 26-week-old male ABHD6-KO mice (Zhao et al., 2014). We also found that 6-week-old ABHD6-KO male mice on chow diet showed no differences in their glucose tolerance compared to wild-type (WT) mice during oral glucose tolerance test (OGTT), despite increased insulin secretion (data not shown) and unaltered insulin sensitivity as revealed by insulin tolerance test (ITT). Unlike

Figure 1. Improved Glucose Tolerance, Insulin Sensitivity, Reduced Food Intake, and Body Weight Gain, and Elevated Muscle and Adipose Glucose Uptake in ABHD6-KO Mice on High-Fat Diet

Male and female ABHD6-KO (homozygous), heterozygous (HZ), and wild-type (WT) mice were maintained on HFD, and food intake and body weight gain were monitored. Oral glucose tolerance test (OGTT) was performed after 8 weeks, after a 6-hr food deprivation. Tail blood was collected at indicated times and analyzed for glucose and insulin by ELISA. Insulin tolerance test (ITT) and hyperinsulinemic euglycemic clamp (HIEC) were performed after 10 weeks on HFD.

(A) Glycemia during OGTT on male WT, HZ, and KO mice (n = 9). Inset depicts area under the curve (AUC) for glycemia.

(B) Insulinemia during OGTT in male mice. Inset, area under the curve.

(C) Glycemia during ITT on male mice (n = 6). Inset depicts area above the curve (AAC).

(D) Glycemia during OGTT on female mice (n = 8). Inset depicts area under the curve.

(E) Corresponding plasma insulin levels for female mice.

(F) Blood glucose levels during ITT on female mice (n = 8). Inset depicts area above the curve for insulinemia.

(G) Blood glucose levels during HIEC on male WT (n = 8), HZ (n = 9), and KO (n = 10) mice.

(H) Glucose infusion rate (GIR) during HIEC on male mice.

(I) Body weight gain of male WT, HZ, and KO mice (n = 9).

(J) Cumulative food intake of male mice over 7 weeks.

(K) Body weight gain in female mice (n = 9).

(L) Cumulative food intake in female mice over 7 weeks.

(M–P) Glucose uptake in muscle and fat tissue. Soleus muscle and visceral fat from ABHD6-KO and WT mice fed HFD for 12 weeks were removed and used for measuring glucose uptake with [^{3}H]-2-deoxy-glucose (2DG), in the absence or presence of insulin (100 nM), as detailed in Experimental Procedures. (M) Glucose uptake in visceral fat of male mice. (N) Glucose uptake in soleus muscle of male mice. (O) Glucose uptake in visceral fat of female mice. (P) Glucose uptake in soleus muscle of female mice.

*p < 0.05 versus WT. *p < 0.05; **p < 0.01 versus WT. See also Table S1 and Figure S1.

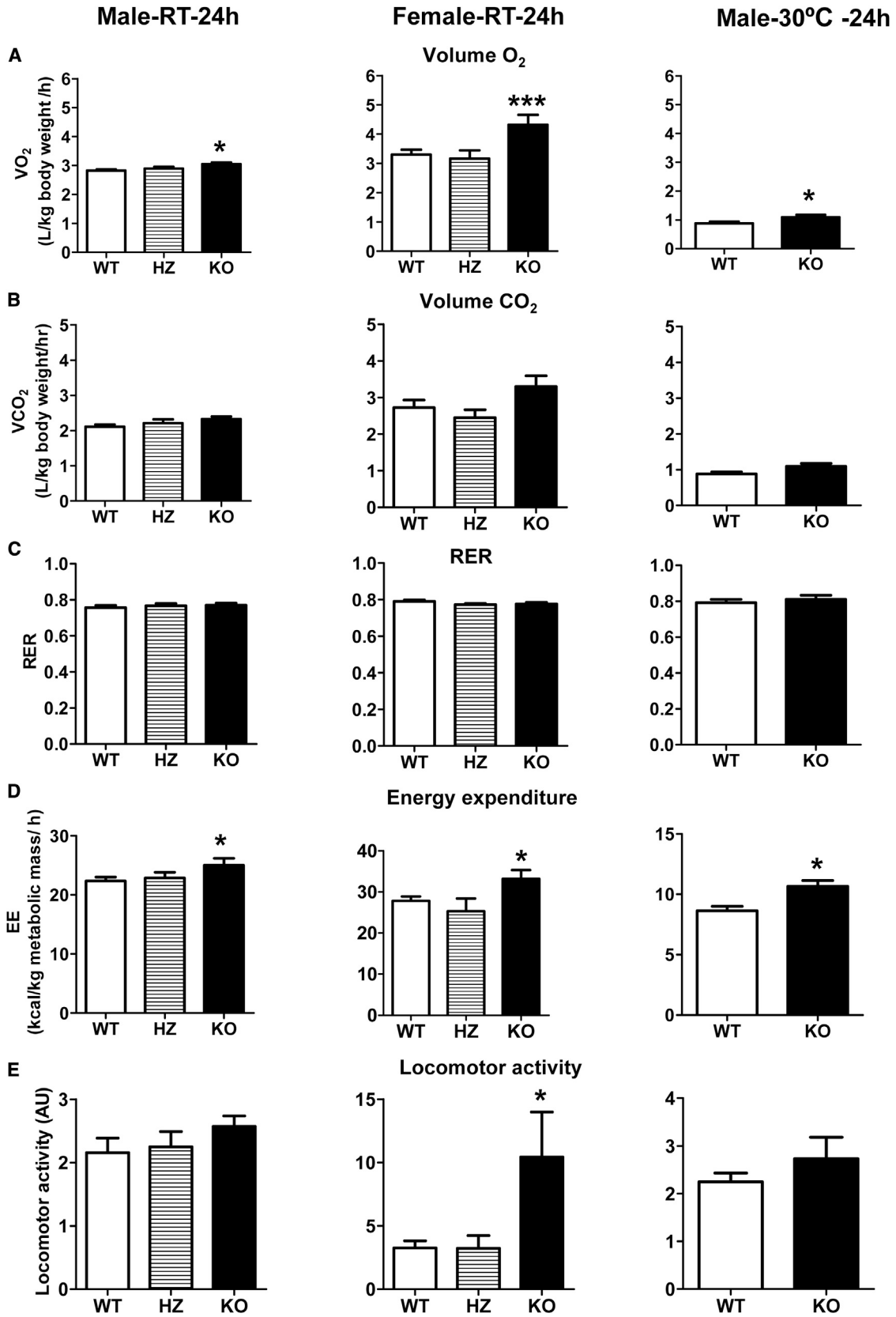

(legend on next page)

male KO mice, female ABHD6-KO mice on chow diet showed slightly reduced body weight gain over 3–24 weeks of age and cumulative food intake over 5–16 weeks of age and displayed better glucose tolerance than WT mice but with reduced insulin secretion during OGTT, indicating that female KO mice are more insulin sensitive, which was confirmed by ITT (data not shown). Overall, female ABHD6-KO mice show a more pronounced phenotype than the males on chow diet.

Ex vivo analysis indicated that visceral fat and soleus muscle from ABHD6-KO mice show enhanced glucose uptake under basal and insulin-stimulated conditions and that insulin action per se is not enhanced (Figures 1M–1P). These effects were more pronounced in female mice (Figures 1O and 1P). Thus, ABHD6 deficiency is associated with enhanced insulin independent glucose uptake by muscle and adipose tissues that likely contributes to improved glucose disposal in the KO mice.

Reduced Fat Mass and Liver Steatosis in ABHD6-KO Mice

Echo-MRI of ABHD6-KO mice revealed no difference in lean mass (Figures S1A and S1E). Fat mass (Figures S1B and S1F) was markedly decreased in female KO mice and modestly in males. Liver weight showed significant reduction in the KO mice as compared to WT mice in both males (Figure S1C) and females (Figure S1G), and this may be related to decreased fat content, as noticed in liver histology, showing more fat accumulation in the WT than KO mice (Figure S1I). In fact, liver TG content was decreased in both female and male KO mice on HFD, as compared to WT mice (Figures S1J and S1K). There was no change in visceral fat weight in male KO mice (Figure S1D) while in female KO mice this was reduced by ~40% (Figure S1H) and was visually evident (Figure S1L).

Blood Chemistry and Additional Parameters of ABHD6-KO Mice

ABHD6-KO mice on HFD showed reduced glycemia and insulinemia. On normal diet, neither glycemia nor insulinemia was different between KO and WT mice (Table S1). There were no differences in plasma glycerol, triglyceride, free fatty acids, or free and total cholesterol levels in chow or HFD-fed KO versus WT mice (Table S1). Rectal temperature of female KO mice was slightly (not significant) higher than WT mice, suggestive of elevated energy expenditure (see below). The growth characteristics of ABHD6-KO mice were not altered as indicated by their body and tail length in comparison to WT mice. Fur appearance was also not different (Figure S1L). We measured various adipokines, cytokines, and hormones in plasma by "protein array" in HFD mice (Figures S1M and S1N) and only six of them showed significant changes (Figure S1M). Fibroblast growth factors (FGF21 and FGF), which are implicated in protection from obesity-mediated complications (Kharitonenkov and Adams, 2014; Owen et al., 2014), were elevated in the plasma of KO mice, whereas proteins related to insulin resistance including ICAM-1, IGFBP-1, and resistin were decreased. RAGE, indicative of inflammation, was also reduced.

Elevated Respiration, Energy Expenditure, and Locomotor Activity in ABHD6-KO Mice

ABHD6-KO mice were acclimatized for 48 hr in metabolic cages either at room temperature or at 30°C (thermoneutral conditions), and measurements were made on the subsequent 24-hr period (third day). Respiratory measurements indicated elevated VO_2 during light and dark phases (data not shown) and during the last 24-hr period (Figure 2A) both in male and female mice, at both room temperature and 30°C. VCO_2 and respiratory exchange ratio (RER) were not affected (Figures 2B and 2C). Energy expenditure as a function of metabolic mass (lean mass + 0.2 × fat mass) was higher in both female and male ABHD6-KO mice, in both the dark and light phases, last 24 hr, and at both temperatures (Figures S2A and 2D).

ABHD6-KO mice show increased locomotor activity over a 24-hr time period (Figure 2E) and during dark phase, and this increase was more marked in females (Figure S2B). In order to determine whether increased locomotor activity is due to changes in anxiety, mice were tested in the elevated-plus maze and open-field tests. Further, we used the Porsolt forced swim test to verify whether ABHD6-KO affects depressive-like behavior, a secondary effect sometimes associated with appetite suppression. No differences were observed between WT and KO mice for any of these parameters (Figures S2C–S2E), suggesting that the enhanced locomotor activity of KO mice is due to voluntary exercise.

Enhanced BAT Function and WAT "Browning" in ABHD6-KO Mice

As ABHD6-KO mice on HFD show enhanced energy expenditure, we examined whether BAT function is elevated in these mice and whether white adipose undergoes "browning." We measured in female ABHD6-KO mice thermogenic gene expression in BAT and genes associated with adipose browning in visceral and inguinal WAT. UCP1, PGC1α, PRDM16, PPARα, and CD36 mRNA levels (Figures 3A–3E) were elevated in visceral

Figure 2. Increased Energy Expenditure and Locomotor Activity in High-Fat-Diet-Fed ABHD6-KO Mice

Male and female ABHD6-KO, HZ, and WT (n = 10) mice were fed HFD for 6 weeks, and at the end of feeding period the mice were placed in metabolic cages at room temperature for 3 days. After acclimatization for the first 2 days, volume of O_2, CO_2 as well as locomotor activity measurements were made on the third day, and, based on these parameters, respiration exchange ratio (RER) and energy expenditure (EE) were calculated. In parallel, metabolic cage measurements were also made with HFD-fed male ABHD6-KO and WT mice under thermoneutral (30°C) conditions (n = 7). Results shown were calculated for the 24-hr period on the third day.

(A) Volume O_2.

(B) Volume CO_2 (expressed as liters/kg body weight/hr).

(C) RER.

(D) Energy expenditure (expressed as kcal/kg metabolic mass/hr).

(E) Locomotor activity (arbitrary units). Metabolic mass was calculated as lean mass + 0.2 × fat mass for each mouse.

*$p < 0.05$; ***$p < 0.001$ versus WT. See also Figure S2.

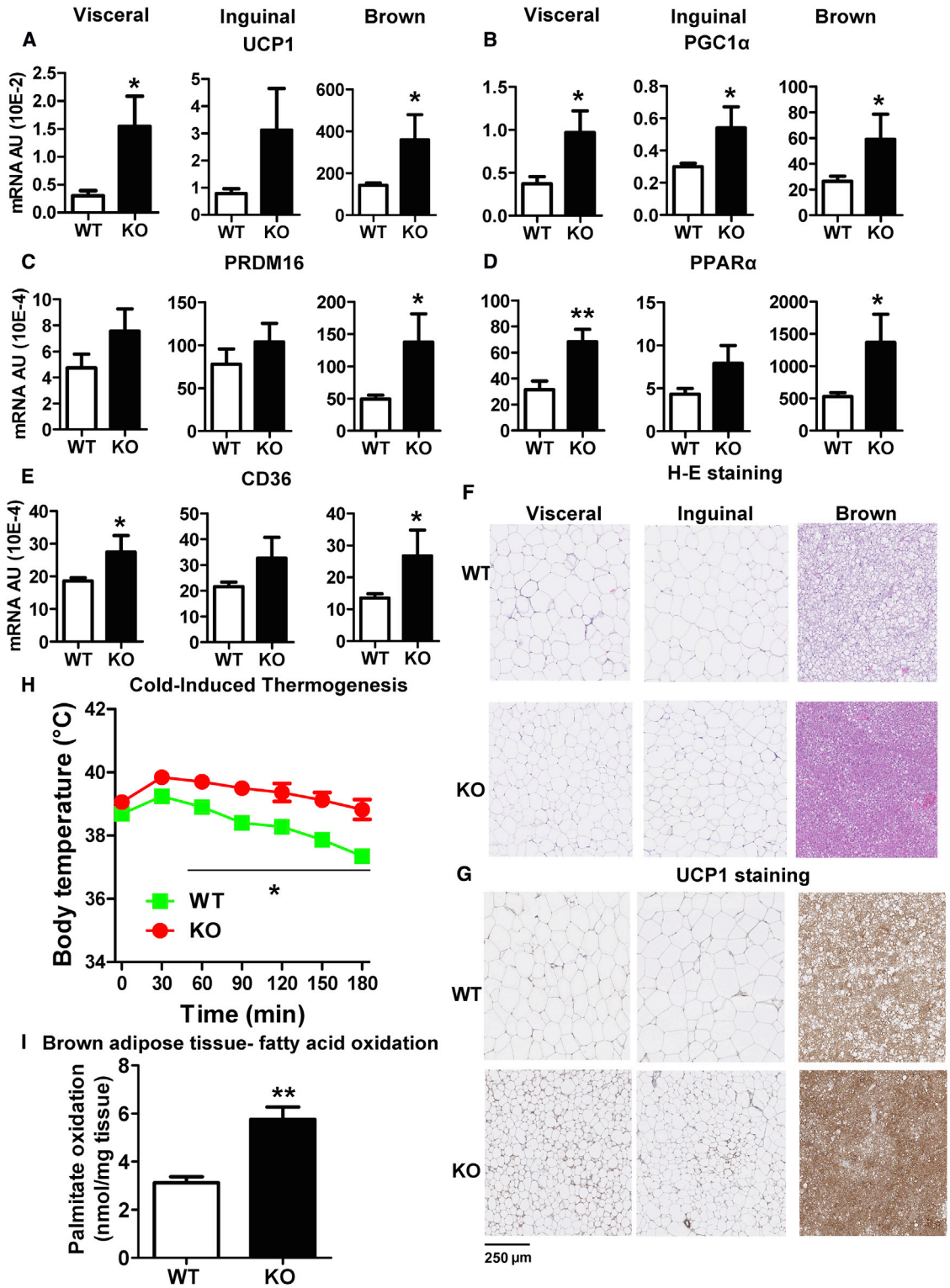

Figure 3. Increased Expression of UCP1 and Other Adipose Browning-Related Genes, Cold-Induced Thermogenesis, and Brown Adipose Fatty Acid Oxidation in HFD-Fed ABHD6-KO Mice

(A–E) Female ABHD6-KO (n = 7) and WT (n = 7) mice fed HFD for 10 weeks were sacrificed, and visceral, inguinal, and brown fat tissues were removed for analysis. Total RNA was extracted, and the expression of various browning marker genes was assessed by RT-PCR. All gene expressions are normalized to 18S RNA expression.

(legend continued on next page)

and inguinal WAT and in BAT from female KO mice. Expression of other browning-related genes (TBX1, CD137, TMEM26, Cox8b, Cox7a1, CIDEA) (data not shown) showed moderate or no change. Expression of PPARα, which controls UCP1 transcription (Xue et al., 2005), was elevated in WAT and BAT (Figure 3D), but no significant changes were seen in PPARβ or PPARγ (data not shown). PPARα target genes CD36 (Figure 3E) and CPT-1 (data not shown) showed increased expression in the KO mice. Histology revealed smaller adipocytes in the visceral and inguinal adipose tissues and smaller adipocytes with much less lipid deposits in the BAT of the ABHD6-KO mice (Figure 3F). UCP1 protein staining was higher in visceral, inguinal, and brown adipose tissues of KO mice (Figure 3G). UCP1 protein levels, quantified from western blots, increased in KO mouse WAT and BAT (Figures S3A–S3C). Cold (4°C)-induced thermogenesis for 3 hr revealed higher ability of the KO mice to maintain their body temperature (Figure 3H), and UCP1 protein levels in these cold-exposed WT and ABHD6-KO mice also showed significant increase (Figures S3D and S3E). Similar gene expression changes were noticed in WAT and BAT from ABHD6-KO mice after 3-day acclimatization at 30°C, except that PPARγ induction was more apparent (Figures S4A–S4H). The elevated UCP1 protein levels seen in both WAT and BAT of ABHD6-KO mice at room temperature conditions were also found to be increased under thermoneutral conditions (Figures S4B and S4C). BAT from KO mice showed nearly 2-fold increase in β-oxidation (Figure 3I). Thus, there is increased thermogenic program and function in BAT and induction of browning-related genes in visceral and subcutaneous adipose tissues of the ABHD6-KO mice.

Pharmacological Inhibition or ASO Knockdown of ABHD6 Triggers Adipose Browning

Administration of ABHD6 inhibitor WWL70 or ABHD6-ASO was shown to protect mice from DIO (Thomas et al., 2013). In order to examine whether pharmacological inhibition of ABHD6 induces adipose browning as seen in ABHD6-KO mice, C57Bl6N mice on HFD (45% calories from fat; 8 weeks) were treated daily with WWL70. Administration of WWL70 elevated UCP1 (Figure 4A) and induced other browning-related genes (Figures 4B–4D) in the visceral adipose. Expression of Cidea and Cox7a1 showed marginal increase, whereas UCP2, PPARα, and PPARγ were unaltered in WWL70-treated mice (data not shown).

ABHD6-ASO-treated mice on 45% HFD showed markedly reduced ABHD6 expression in visceral adipose in association with induction of UCP1, PRDM16, PPARα, and PPARγ (Figures 4E–4I). Expression of Cox7a1, Elovl3, TBX1, and TMEM26 were also elevated in the ABHD6-ASO-treated mice, whereas Cidea expression did not change (Figures 4J–4N). Similar to ABHD6-KO mice, ASO-treated mice maintained their body temperature in cold better than controls and the area above the curve indicated significantly lower decline in body temperature in the ABHD6-ASO-treated mice (Figure 4O). Thus, in vivo inhibition or knockdown of ABHD6 causes WAT browning as seen in the KO mice.

ASO Knockdown of ABHD6 in Differentiated 3T3-L1 Cells Induces Browning-Related Gene Expression

We further examined whether the adipose browning-inducing effects of ABHD6-ASO are cell autonomous using 3T3-L1 preadipocytes after differentiation. Treatment of fully differentiated 3T3-L1 cells with ABHD6-ASO for 24 hr led to decreased mRNA levels of ABHD6 and elevated expression of UCP1, PGC1α, PRDM16, PPARα, and TMEM26 (Figures 4P–4V). These results are consistent with the view that ABHD6 ASO knockdown effects on browning are cell autonomous.

ABHD6 Inhibition and 1-MAG Cause Adipose Browning via PPARα and PPARγ in a Cell-Autonomous Manner

To gain insight into the mechanism by which ABHD6 inhibition causes WAT browning, we first verified whether 1-MAG hydrolase activity is lowered in the adipose tissues of ABHD6-KO mice, which also contain the classical MAG lipase (Taschler et al., 2011). Total 1-MAG hydrolase activity in extracts of visceral and brown adipose tissues from the KO mice was markedly decreased (Figure 5A) indicating that ABHD6 contribution to MAG hydrolysis in these adipose tissues is significant. MAG hydrolase activity in inguinal adipose was not altered (Figure 5A). The decreased MAG hydrolase activity in WAT and BAT was reflected in elevated 1-MAG species in these adipose tissues (Figures 5B and 5C). Changes in 2-MAG levels were modest (data not shown), similar to our earlier report in ABHD6-KO mouse islets (Zhao et al., 2014). Normalization of MAG levels as a function of total tissue protein yielded similar pattern (data not shown).

We examined whether the effects of ABHD6 suppression are cell autonomous and intrinsic to adipocyte and whether 1-MAG acts as a signal for browning. Incubation of differentiated 3T3-L1 mouse adipocytes with WWL70, 1-oleoylglycerol, or 1-palmitoylglycerol increased expression of the browning marker UCP1 and PPARα (Figure S5A). Similar changes were noticed with WWL70 and 1-oleoylglycerol in differentiated human primary preadipocytes (Figure 5D). Addition of the PPARα antagonist GW6471 completely abrogated the WWL70 and 1-oleoylglycerol-induced increases in UCP1 and PPARα expression (Figure 5D), suggesting that the browning changes seen in WAT by ABHD6 suppression are mediated by1-MAG in a cell-autonomous manner, at least in part via activation of PPARα. WWL70 and 1-oleoylglycerol-stimulated respiration in 3T3-L1 adipocytes (Figures S5B–S5E) and human preadipocytes (Figures S5F–S5H), likely because of increased UCP1-mediated uncoupled O_2 consumption (Figures 5E, S5E, and S5F). Similar to UCP1 expression, this increased O_2 consumption was curtailed by GW6471 (Figures 5E, S5B, and S5E).

(F and G) Histological (H&E staining) and immunochemical (for UCP1 expression) examination on the adipose tissues.
(H) Another batch of HFD-fed ABHD6-KO and WT mice were placed in cold room (4°C) for 3 hr, and cold-induced thermogenesis was evaluated by measuring rectal temperature.
(I) Fatty acid oxidation using [1-^{14}C]-palmitate measured in brown adipose tissue from mice fed a HFD.
*$p < 0.05$; **$p < 0.01$ versus WT. See also Figures S3 and S4.

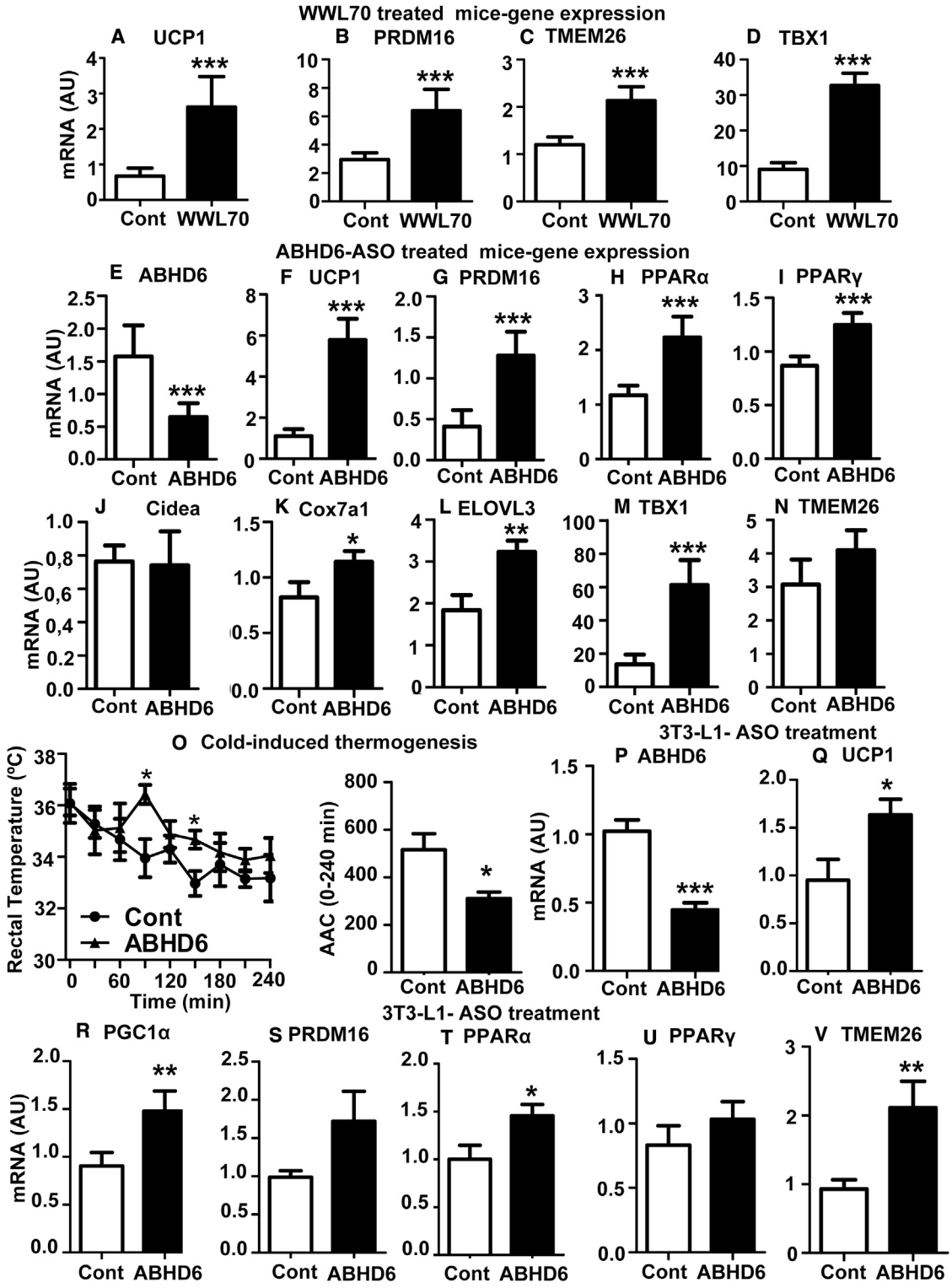

Figure 4. Suppression of ABHD6 by WWL70 or Antisense-Oligonucleotide Increases Expression of Browning-Related Genes in White Adipose Tissue, Differentiated 3T3-L1 Cells, and Cold-Induced Thermogenesis in HFD-Fed Mice

Wild-type C57Bl6N mice fed high-fat diet for 8 weeks were treated with WWL-70 (10 mg/kg/day, i.p.) or vehicle (n = 9 for each group) or ABHD6-ASO (25 mg/kg/2 weeks) or control ASO (n = 9 for each group), during the feeding period. Cold-induced thermogenesis was assessed in ABHD6-ASO-treated mice at the end of the 8-week period. After the feeding period, mice were sacrificed, and visceral fat was removed and processed for measuring the expression of UCP1

(legend continued on next page)

Transactivation experiments revealed that 1-oleoylglycerol and 1-palmitoylglycerol could activate PPARα-driven luciferase gene expression, similar to PPARα agonist WY14643 (Figure 5F). There was also significant transactivation of PPARγ, but not PPARβ, by 1-MAG (Figure 5F). We verified the binding ability and affinity of 1-MAG to PPARα and PPARγ using PPAR-GAL4 binding assay, where the ligand binding domain of PPAR is fused with GAL4 DNA binding domain and the expression of a reporter gene is followed. Results showed that while the synthetic ligands WY14643 and rosiglitazone showed high affinity to bind and activate PPARα and PPARγ as expected (Figures S6A and S6D), both 1-OG and 1-PG were also able to bind and activate these PPARs with an EC_{50} of 10–19 μM, which is within their physiological range of intracellular concentrations (Figures S6B, S6C, S6E, and S6F). Finally, preadipocytes from ABHD6-KO mice expressed high levels of UCP1 and PPARα after differentiation as compared to WT preadipocytes, an effect that was abrogated by PPARα antagonist GW6471 (Figure 5G).

We further examined the contribution of PPARγ to 1-MAG-mediated browning. PPARγ antagonist T0070907 led to suppression of WWL70 or 1-oleoylglycerol-mediated increase in the expression of UCP1 and other browning-related genes in human differentiated preadipocytes (Figure 5H). Overall, the data support the view that 1-MAG mediates the adipocyte browning induced by ABHD6 suppression in a cell-autonomous manner, probably involving PPARα and PPARγ activation.

Pair Feeding Does Not Prevent ABHD6-KO-Mediated Protection from HFD-Induced Obesity, Glucose Intolerance, and Insulin Resistance

Since ABHD6-KO mice on HFD exhibited slightly reduced food intake, we verified whether this could explain the observed effects on body weight gain, glucose tolerance, and insulin sensitivity. After ABHD6-KO and WT mice were pair fed for 2 weeks, body weight gain was still lower in ABHD6-KO mice (Figures 6A and 6B). Similarly, OGTT revealed improved glucose tolerance and ITT showed better insulin sensitivity (Figures 6C–6E) in the ABHD6-KO mice compared to the pair-fed WT mice. The increased UCP1 protein content seen in WAT and BAT of ad libitum HFD-fed ABHD6-KO mice was also noticeable in pair-fed mice (Figures 6F–6I), suggesting that the beneficial changes in glucose/insulin homeostasis seen in the KO mice cannot be fully accounted for by changes in food intake.

PPARα Antagonism Counteracts Adipose Browning, Thermogenic Program, and Beneficial Metabolic Effects in ABHD6-KO Mice

Treatment of HFD-fed ABHD6-KO male mice with the PPARα antagonist GW6471 slightly elevated their body weight gain (Figure 7A), without altering food intake (Figure 7B). Even though glycemia during OGTT was not changed (Figure 7C), insulinemia showed a tendency to increase (Figure 7D) revealing lower insulin sensitivity, and this was confirmed in ITT (Figure 7E). PPARα antagonism lowered oxygen consumption and VCO_2 in the ABHD6-KO mice, without change in RER (Figures S7A–S7C). The elevated energy expenditure in KO mice, measured at 30°C, was reduced by GW6471 treatment (Figure 7F). This decreased energy expenditure was associated with curtailed expression of UCP1 (Figure 7G) and other browning-related genes in BAT and WAT (Figures S7E–S7G), indicating that in ABHD6-KO mice PPARα mediates adipose browning and thermogenic reprogramming at least partially. Interestingly, the increased locomotor activity seen in ABHD6-KO mice was also curtailed by PPARα antagonism (Figure S7D). The elevated β-oxidation in BAT of ABHD6-KO mice was also normalized to WT levels by PPARα antagonist treatment (Figure S7H).

DISCUSSION

We previously demonstrated the regulatory role of ABHD6 and 1-saturated monoacylglycerol in insulin secretion by pancreatic β cells and identified Munc13-1 as the intracellular receptor for MAG-induced exocytosis (Zhao et al., 2014, 2015). The present results indicate roles for ABHD6 in whole-body energy homeostasis that are of interest for metabolic disorders. When fed HFD the ABHD6 KO mice show (1) reduced body weight gain; (2) protection from hepatic steatosis; (3) a modest lowering of food intake; (4) improved glucose tolerance; (5) increased insulin sensitivity and protection from hyperinsulinemia; (6) enhanced insulin-independent glucose uptake in adipose and muscle; (7) increased locomotor activity, females being more responsive; (8) elevated energy expenditure; (9) augmented fatty acid oxidation in BAT; (10) increased cold-induced thermogenesis; (11) browning of WAT; and (12) increased plasma FGF21, which antagonizes metabolic-syndrome-related defects and activates BAT and beige adipocytes (Hondares et al., 2011a; Owen et al., 2014). Heterozygous mice, partially deficient in ABHD6, showed an intermediate phenotype between WT and KO mice for many parameters, revealing a gene dosage effect. Also several of these effects, in particular, adipose browning and cold-induced thermogenesis, were replicated in vivo by the ABHD6 inhibitor WWL70 and by ABHD6-ASO. Thus, the results demonstrate that ABHD6 is a key player in the control of energy homeostasis and in the regulation of BAT function and white adipose browning. Recently, it has been observed that ASO directed against ABHD6 causes elevated energy expenditure and protects male mice against HFD-induced obesity, hepatic steatosis, and systemic insulin resistance, but the underlying

and browning-related genes normalized to 18S RNA. In order to assess the effect of ABHD6 suppression by ASO in fully differentiated 3T3-L1 cells, the cells after differentiation were treated with control- or ABHD6-ASO for 24 hr. Then, the cells were harvested for gene expression analysis by RT-PCR.

(A–D) Browning-related gene expression in visceral adipose from WWL70-treated and control mice. (A) UCP1, (B) PRDM16, (C) Tmem26, and (D) TBX1.

(E–N) Browning-related gene expression in visceral adipose from control-ASO and ABHD6-ASO-treated mice: (E) ABHD6; (F) UCP1; (G) PRDM16; (H) PPARα; (I) PPARγ; (J) Cidea; (K) Cox7a1; (L) ELOVL3; (M) TBX1; and (N) TMEM26.

(O) Cold-induced thermogenesis in ABHD6-ASO-treated and control mice and the area above the curve for temperature curves.

(P–V) Gene expression in 3T3-L1 cells treated with control- or ABHD6-ASO. (P) ABHD6; (Q) UCP1; (R) PGC1α; (S) PRDM16; (T) PPARα; (U) PPARγ; and (V) TMEM26. *$p < 0.05$; **$p < 0.01$; ***$p < 0.001$, compared to corresponding controls; n = 10 for each group.

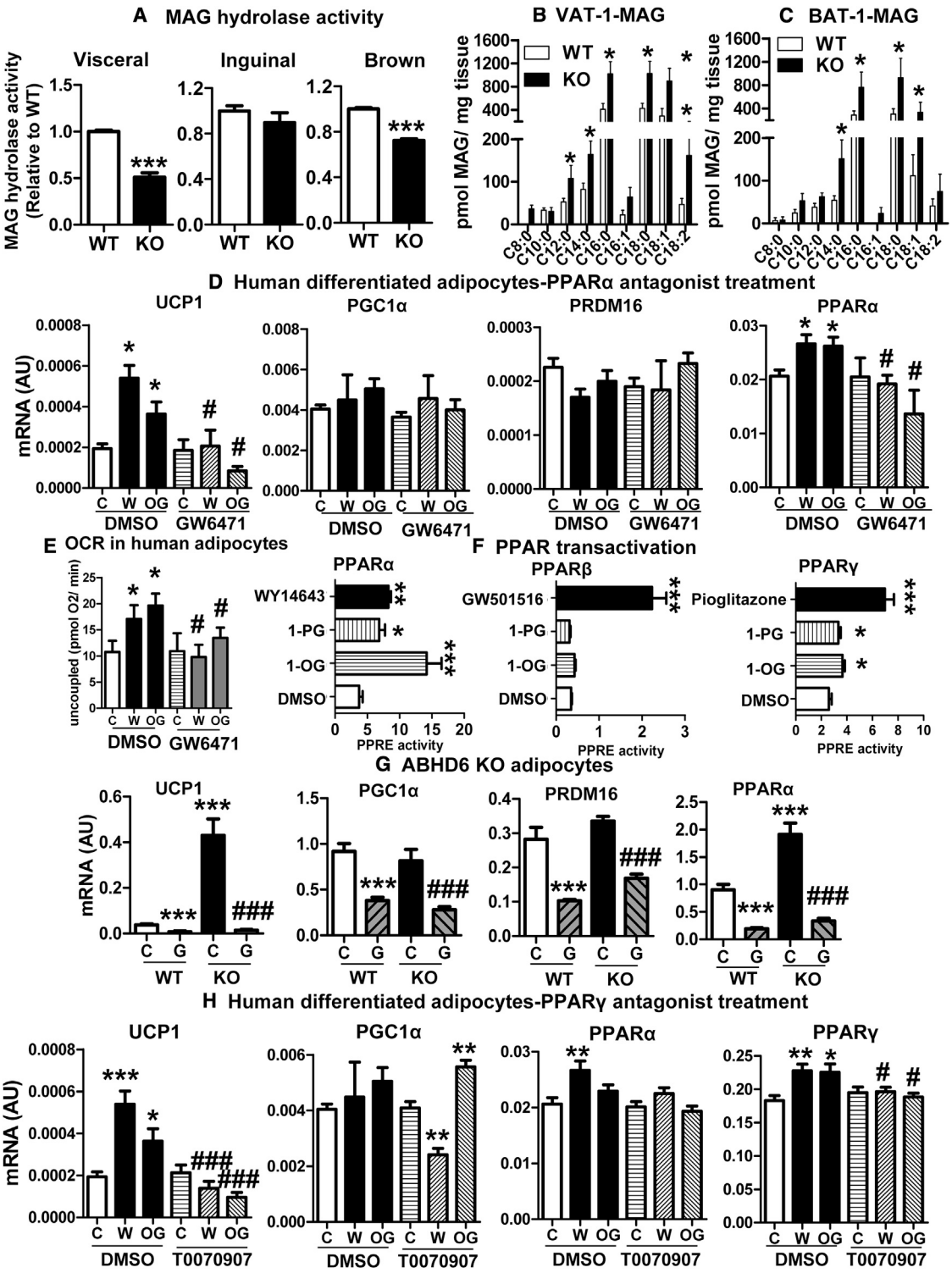

Figure 5. Accumulation of 1-MAG in ABHD6-KO Mouse Adipose Tissues and PPARα and PPARγ Dependence of Elevated Browning Gene Expression by 1-MAG and WWL70 in Human Adipocytes or in ABHD6-KO Mouse Adipocytes

(A) MAG hydrolase activity in visceral, inguinal, and brown adipose tissues from ABHD6 WT and KO mice. Adipose tissues were employed for assaying MAG hydrolysis activity using 1-S-arachidonoylglycerol. *p < 0.05 versus WT (n = 7, each).

(B and C) Visceral and brown adipose tissues were processed for MAG species analysis. (B) Increased levels of long-chain 1-MAG species in visceral adipose isolated from HFD-fed female ABHD6-KO mice. *p < 0.05 versus WT mice (n = 7, each). (C) Increased levels of long-chain 1-MAG species in brown adipose isolated from HFD-fed female ABHD6-KO mice (n = 7, each). *p < 0.05 versus WT.

(legend continued on next page)

mechanism was not known (Thomas et al., 2013). The present data provide that ABHD6-ASO induces WAT browning and BAT activation, which contribute to the protective effect seen in HFD mice. This comprehensive study of both males and female mice on normal or high-fat diet considerably extends our understanding of the role of ABHD6 and lipolysis-derived 1-MAG signaling in fuel homeostasis.

The mechanism whereby ABHD6 suppression exerts beneficiary metabolic effects is likely multifactorial. The slight reduction in food intake alone cannot quantitatively explain all metabolic improvements. Thus, food intake was similarly reduced by ~8% in male and female mice, yet the phenotype in females for glucose tolerance, body weight gain, fat mass, and insulin sensitivity was more pronounced. In addition, the protective effects of ABHD6-KO persist in the context of pair feeding, indicating that the lower food intake is not primarily responsible for the improved metabolic outcomes observed in ABHD6-KO mice. The underlying causes for the modestly lowered food intake in the KO mice are not clear. Central ABHD6 involvement is a possibility; however, a decrease in ABHD6 activity is expected to increase the endocannabinoid 2-arachidonoylglycerol that in fact enhances appetite (Di Marzo and Matias, 2005), which is not the case in the KO mice. Also, ABHD6 ASO, which does not lower brain ABHD6 levels, caused similar metabolic effects (Thomas et al., 2013); central involvement cannot explain the reduced appetite and metabolic effects in the KO mice. Also, recently it has been shown that ABHD6 inhibition in vivo by WWL70 had no effect on brain 2-AG levels (Alhouayek et al., 2013), indicating that ABHD6 suppression mediates its effects largely independent of central involvement. At least part of the beneficiary effects of ABHD6-KO on glycemia could be due to the enhanced insulin-independent glucose uptake both in skeletal muscle and adipose tissues, and this, in turn, could contribute to decreased body demand for insulin and thus to reduced hyperinsulinemia that drives obesity (Wiernsperger, 2005a, 2005b).

However, an important contributor to the beneficiary effect of ABHD6 deletion is likely enhanced BAT function and also WAT browning. Thus, energy expenditure was increased in KO mice during the light phase when the animals did not show any difference in locomotor activity. Furthermore, energy expenditure was elevated at 30°C thermoneutral conditions, indicating that these effects are not because of room-temperature-mediated stimulation of BAT and also not due to any skin or fur defects as pointed out recently (Nedergaard and Cannon, 2014). In addition, cold-induced thermogenesis was enhanced in both ABHD6-KO and ABHD6-ASO-treated mice. It is also important to point out that, while subcutaneous adipose was considered to be the prime target of browning in other mouse models, we find that predominant changes in browning-related gene expression are noticeable in visceral WAT in ABHD6-KO mice.

Little is known about the biochemical basis of WAT browning. Several transcriptional regulators including PPARs and co-activators PRDM16 and PGC1α are known to be involved in the conversion of WAT to brite adipose (Richard et al., 2010; Rosen and Spiegelman, 2014). However, whether metabolic pathways or signals play a role in this process is unknown. The results support the view that 1-MAG signaling can drive intrinsic and cell-autonomous adipose browning in part via PPARα and PPARγ activation and that ABHD6 regulates adipose browning by controlling the signal competent 1-MAG levels. The evidence is as follows: (1) various 1-MAG species are increased in visceral adipose of ABHD6-KO mice; (2) 1-MAG, WWL70, and ABHD6-ASO induce UCP1 and PPARα in differentiated 3T3L1 preadipocytes and human preadipocytes; (3) PPARα and PPARγ antagonists abrogate UCP1 induction by 1-MAG and ABHD6 inhibition in adipocytes; (4) UCP1 expression is dramatically induced during differentiation of preadipocytes from ABHD6-KO WAT, and this is completely abolished by PPARα antagonism; (5) 1-MAG can activate PPARα and PPARγ directly by binding to the ligand binding domain of these transcription factors; (6) PPARα and PPARγ target genes are induced in ABHD6-KO WAT; (7) 1-MAG and WWL70 increase uncoupled respiration in 3T3L1 preadipocytes and human adipocytes, and this is blocked by a PPARα antagonist; (8) PPARα antagonist treatment of ABHD6-KO mice prevents the browning phenomenon and associated metabolic changes; and (9) treatment of mice with ABHD6-ASO or WWL70 induces WAT browning similar to ABHD6-KO. However, considering that PPARs are necessary for UCP1 expression per se, and that the PPARα antagonist also decreased UCP1 expression in the WAT and

(D) PPARα dependence of elevated browning gene (UCP1, PGC1α, PRDM16, and PPARα) expression by 1-oleoylglycerol or WWL70 in human adipocytes. Fully differentiated human adipocytes were incubated overnight with either DMSO vehicle (control, C), 10 μM WWL70 (W), or 100 μM 1-OG (OG), in the presence and absence of PPARα antagonist 1 μM GW6471, and the cells were collected for mRNA analysis. Results were normalized to 18S RNA (n = 5). *p < 0.05 versus control (DMSO); #p < 0.05 versus GW6471.

(E) Stimulation of uncoupled oxygen consumption rate (OCR) in differentiated human adipocytes by 1-OG and WWL70, and this increase is curtailed by PPARα antagonist GW6471 (n = 5). *p < 0.05 versus DMSO control; #p < 0.05 versus GW6471. For further details, see Figure S4E.

(F) Transactivation of PPARα and PPARγ by 1-MAG. PPAR transactivation assay was done in 293T cells, transfected with plasmids expressing PPARα, PPARβ, or PPARγ, using dual luciferase PPRE reporter assay. WY14643, GW501516, and pioglitazone were used as positive controls for the activation of PPARα, PPARβ, and PPARγ, respectively (n = 6). *p < 0.05, **p < 0.01, ***p < 0.001 versus DMSO.

(G) PPARα antagonist GW6471 suppresses the expression of browning-related genes UCP1, PGC1α, PRDM16, and PPARα in adipocytes differentiated ex vivo from pre-adipocytes isolated from chow-diet-fed ABHD6-KO and WT mice. C, DMSO control; G, GW6471 treated. ***p < 0.001 versus WT-DMSO; ###p < 0.001 versus KO-DMSO (n = 5).

(H) PPARγ dependence of elevated browning gene (UCP1, PGC1α, PPARα, and PPARγ) expression by 1-oleoylglycerol or WWL70 in human adipocytes. Human adipocytes were treated as in (D) overnight with WWL70 or 1-oleoyglycerol in the absence or presence of 1 μM PPARγ antagonist T0070907. Then, the adipocytes were harvested, and mRNA expression of browning-related genes was assessed by RT-PCR. Gene expressions were normalized to 18S RNA.

*p < 0.05; **p < 0.01; ***p < 0.001 versus control (C); #p < 0.05; ###p < 0.001 versus corresponding WWL70 (W) or 1-OG (OG) without T0070907 treatment (n = 5). See also Figure S5.

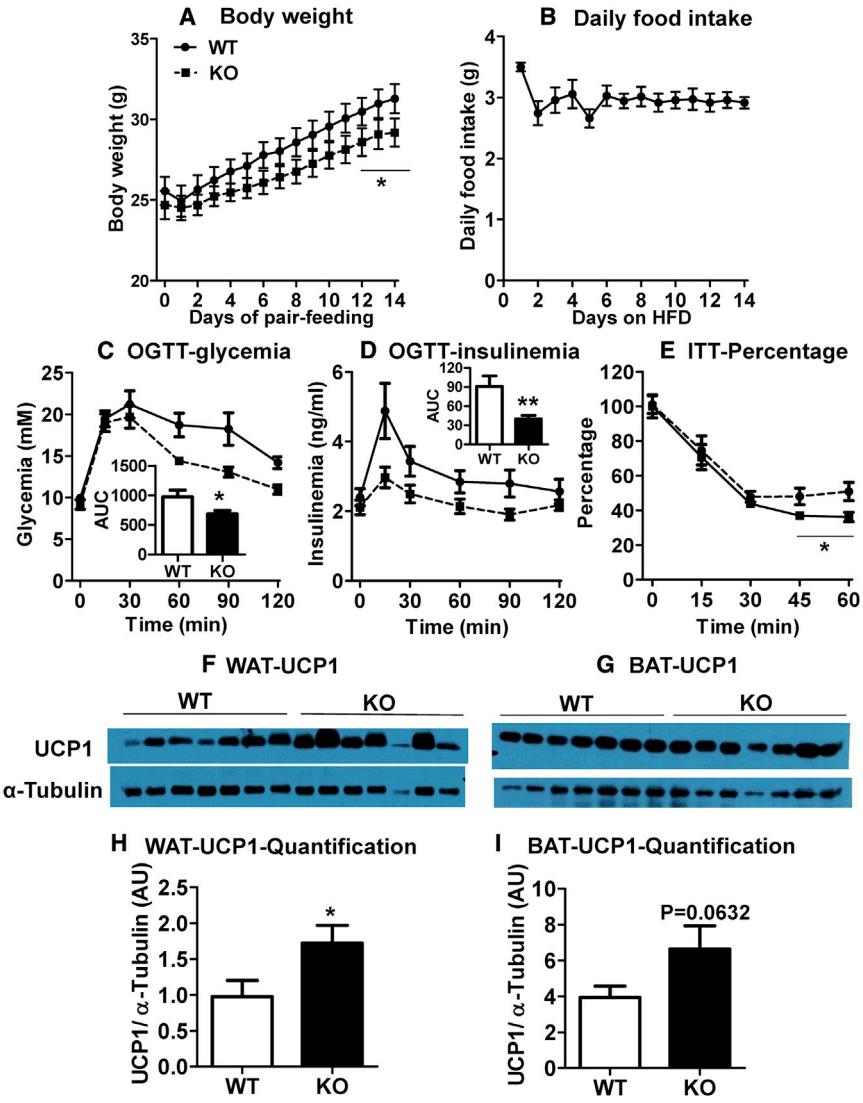

Figure 6. Pair-Fed ABHD6-KO Mice on HFD Also Show Reduced Body Weight, Improved Glucose Tolerance, and Insulin Sensitivity

Male ABHD6-KO and WT mice (6 weeks old) were pair fed HFD. Daily body weight gain was monitored, and OGTT and ITT were performed at the end of the feeding period. Then, the mice were sacrificed, and visceral and brown fat tissues were isolated for western blot analysis of UCP1.

(A) Body weight.

(B) Daily food intake of KO mice; the same amount of food is given to pair-fed WT mice.

(C) Glycemia during OGTT. Inset depicts AUC.

(D) Insulinemia during OGTT. Inset depicts AUC.

(E) ITT. Results of ITT were calculated as percentage of basal (0 min) glycemia.

(F and G) UCP1 protein expression in WAT (F) and UCP1 protein expression in BAT (G).

(H and I) Quantification of UCP1 protein expression in western blots of WAT (F) and BAT (G).

*$p < 0.05$; **$p < 0.01$ versus WT.

BAT of WT mice, additional PPAR-independent mechanisms for 1-MAG-mediated adipose browning and BAT activation are possible.

ABHD6 and 1-MAG also appear to play a role in BAT function, which is important considering that the thermogenic contribution of classical BAT is likely predominant, even under conditions of "WAT browning" (Shabalina et al., 2013). Thus, ABHD6-KO mice showed elevated levels of various 1-MAG species in BAT, whereas 2-MAG did not rise significantly. BAT of the KO mice showed higher fat oxidation and induction of many of the BAT marker genes including PRDM16, PPARα, CD36, PGC1α, and CIDEA. Also, UCP1 level was markedly increased in BAT of the KO mice in association with better cold tolerance despite being leaner. Similar to WAT browning, 1-MAG appears to activate BAT function at least in part through PPARα; however, other mechanisms are possible. This inference is supported by the counteracting effect of PPARα antagonist on UCP1 induction in ABHD6-KO mice.

The phenotype of male and female ABHD6-KO mice was qualitatively similar even though it was quantitatively more marked in females. The reason for this is uncertain, but estrogens are well known to be protective against metabolic syndrome and diabetes (Mauvais-Jarvis et al., 2013; Zhu et al., 2014). Also, BAT in female mice is more efficient in its mitochondrial organization (Nadal-Casellas et al., 2013; Nookaew et al., 2013), which may also contribute to their increased responsiveness to ABHD6 deletion.

Mechanism underlying the elevated locomotor function seen in the ABHD6-KO mice is not clear. Since there is no associated stress or anxiety in the ABHD6-KO mice, and, as the elevated locomotor activity is seen mostly during dark phase, when the rodents are more active, it can be inferred that ABHD6 suppression promotes voluntary exercise. The effects on locomotor function may also be dependent on PPAR activation, as these effects could be suppressed by PPARα antagonist.

Lipolytic products are important physiological activators of both PPARα and PPARγ (Badin et al., 2012; Haemmerle et al., 2011; Mottillo et al., 2012). Several reports indicate the role of PPARγ in WAT browning and BAT function (Ohno et al., 2012; Spiegelman, 2013). Indeed, we noticed that 1-MAG can also activate PPARγ in addition to PPARα, but not PPARβ/δ. Inasmuch as PPARγ antagonist could lower the effectiveness of WWL70 and 1-oleoylglycerol in inducing browning-related gene expression in differentiated human preadipocytes, it appears that PPARγ also plays a role in controlling ABHD6/1-MAG-mediated adipose browning, besides other mechanisms.

The possibility that certain centrally mediated effects play a role in the elevated locomotor activity and in adipose browning and BAT activation cannot be eliminated entirely in the

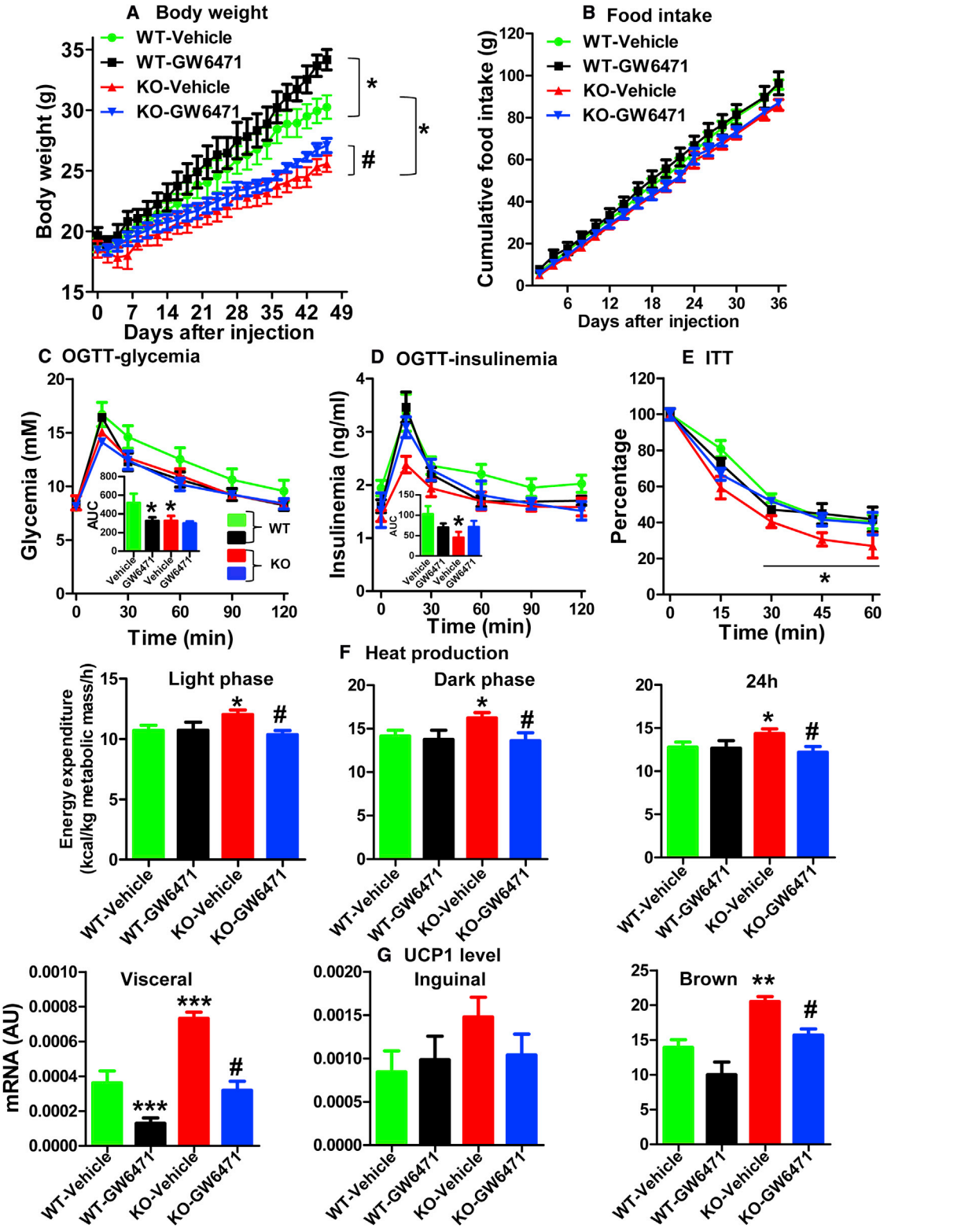

(legend on next page)

ABHD6-KO mice, even though the results from ABHD6-ASO-treated mice do not support this mechanism as ASO does not cross the blood-brain barrier and does not reduce ABHD6 expression in brain (Thomas et al., 2013).

Collectively, our results demonstrate that ABHD6 regulates fuel homeostasis, WAT browning, and BAT function. The mechanism of adipose browning appears to involve 1-monoacylglycerol acting as an intrinsic cell-autonomous signal that causes it beneficial effects in part via PPARα and PPARγ activation in adipose tissues. ABHD6 inhibition may provide a therapeutic approach for both lean and obese T2D. Thus, it was reported earlier that ABHD6 inhibition in the low-dose streptozotocin lean model of T2D restores normal glucose tolerance via enhanced insulin secretion (Zhao et al., 2014). Here, we show in obese mice with hyperglycemia and marked glucose intolerance that ABHD6 deficiency reduces body weight gain and improves glucose homeostasis and insulin action together with mild reduction in appetite and enhanced locomotor activity. Targeting ABHD6 offers a distinct way to develop both anti-obesity and T2D drugs.

EXPERIMENTAL PROCEDURES

Generation and Maintenance of Whole-Body ABHD6-KO Mice

All procedures involving animal studies were approved by the Institutional Committee for the Protection of Animals. Whole-body ABHD6-KO mice were generated on pure C57Bl6N background (Zhao et al., 2014). The mice were maintained individual cages on a standard chow diet (Harlan Teklad, 15% fat by energy) and 12-hr-dark/light cycle at 21°C with free access to water.

Metabolic Studies on High-Fat-Diet-Fed Mice

Male and female wild-type (WT), homozygous ABHD6-KO (KO), and heterozygous (HZ) mice (5 weeks) were placed on chow or high-fat diet (HFD; 60% fat by energy) for 8 weeks (Peyot et al., 2010). Body weight and food intake were monitored each week. At the end of feeding regimen, mice were placed in metabolic cages, for 3 days and O_2 consumption (VO_2), CO_2 production (VCO_2), respiratory exchange ratio (RER), locomotor activity, and energy expenditure by indirect calorimetry were monitored. Energy expenditure was expressed as a function of metabolic mass (lean mass + 0.2 × fat mass) as suggested previously (Even and Nadkarni, 2012). Two days after CLAMS studies, lean and fat mass were determined by echo MRI. Then oral glucose tolerance test (OGTT) was performed.

Hyperinsulinemic Euglycemic Clamp, OGTT, and ITT

Male and female WT, ABHD6-KO, and HZ mice on chow diet or HFD were used for OGTT and ITT (Zhao et al., 2014). Hyperinsulinemic euglycemic clamp (HIEC) was done on male mice fed HFD, and OGTT was performed on male and female mice (Zhao et al., 2014). Intraperitoneal insulin tolerance test (IP-ITT) was performed under fed conditions. Insulin was administered intraperitoneally at a dose of 0.75 U/kg body weight (BW). Blood was collected at different times, and glycemia was monitored.

Cold-Induced Thermogenesis

Female ABHD6-KO and WT mice, maintained on HFD for 12 weeks, were placed in individual cages at 4°C. Rectal temperature was monitored prior to cold exposure and at indicated times during cold exposure for 3 hr.

PPARα Antagonist Treatment of Mice

Female ABHD6-KO and WT mice, kept on HFD for 8 weeks, were given PPARα antagonist GW6471 once every 2 days (1 mg/kg BW) or vehicle, intraperitoneally. Mice were then placed in metabolic cages at thermoneutral condition (30°C), and respiratory exchange ratio, energy expenditure, and locomotor activity were recorded. Then, lean and fat mass of these mice were measured followed by OGTT and ITT. Then, the mice were sacrificed, and visceral, inguinal, and brown fat tissues were isolated for gene expression analysis.

Behavior Tests

Tests for assessing anxiety (elevated plus maze and open field) and depressive behavior (forced swimming) were conducted on ABHD6-KO and WT mice (Sharma and Fulton, 2013).

Treatment of High-Fat-Diet-Fed Mice with ABHD6 Inhibitor

Male mice (6–8 weeks old) were fed 45% fat diet for 8 weeks. Mice received either WWL70 at 10 mg/kg BW/day intraperitoneally or vehicle (controls). After 8 weeks, mice were sacrificed, and visceral fat was processed for UCP1 immunohistochemistry and browning-related gene expression.

Treatment of High-Fat-Diet-Fed Mice with ABHD6 Antisense Oligonucleotide

A 20-mer phosphorothioate antisense oligonucleotide (ASO) against ABHD6 was designed and supplied by ISIS Pharmaceuticals (Thomas et al., 2013). Male mice (6–8 weeks old) were fed a 45% fat diet for 8 weeks. One group of mice was injected with ABHD6-ASO biweekly (25 mg/kg BW), and another group was given control ASO. After 8 weeks, cold-induced thermogenesis at 4°C was assessed and the mice were sacrificed, and visceral fat was processed for measuring browning-related gene expression.

Glucose Uptake and Fatty Acid Oxidation

Glucose uptake was measured using 0.1 mM [^{3}H]-2-deoxyglucose (5 μCi; PerkinElmer) in visceral fat and soleus muscle (Attané et al., 2011), and palmitate oxidation was measured with 1 mM 1-[^{14}C]-palmitate (PerkinElmer) in inguinal fat, visceral fat, brown fat, and soleus muscle (Attané et al., 2012), isolated from ABHD6-KO and WT mice on HFD for 14 weeks.

PPAR Transactivation Assay

293T Cells were transfected with plasmids expressing PPARα, PPARβ or PPARγ, PPAR response element-directed luciferase expression plasmid

Figure 7. Reversal of ABHD6-KO-Mediated Effects on Obesity, Glucose Tolerance, Insulin Sensitivity, Energy Expenditure, and Adipose Tissue UCP1 Expression by PPARα Antagonist

Female ABHD6-KO and WT mice were fed HFD for 8 weeks without or with PPARα antagonist GW6471 treatment (1 mg/kg; once every 2 days, i.p.). Daily body weight gain and food intake were monitored, and, at the end of feeding-period energy expenditure, lean and fat mass were assessed, and OGTT and ITT were performed. Then, the mice were sacrificed, and adipose tissues were isolated for measuring browning-related gene expression.

(A) Body weight.

(B) Food intake.

(C) Glycemia during OGTT. Inset depicts area under the curve (AUC).

(D) Insulinemia during OGTT. Inset depicts AUC.

(E) ITT. Glycemia with time is shown as percentage of basal 0 min value.

(F) Energy expenditure under thermoneutrality (30°C) conditions (expressed as kcal/kg metabolic mass), during light and dark phases and complete 24 hr.

(G) UCP1 expression in visceral, inguinal, and brown adipose tissues (n = 6, each group).

*p < 0.05, **p < 0.01, ***p < 0.001 versus WT-Vehicle; #p < 0.05 versus KO-Vehicle. See also Figure S5.

(PPRE X3-TK-luc) and Renilla luciferase control plasmid. The transfected cells were starved overnight in DMEM without FBS and incubated in FBS-free DMEM with 10 μM WWL70, 100 μM 1-palmitoylglycerol, 100 μM 1-oleoylglycerol, 50 μM WY14643, 100 nM GW501516, 50 μM pioglitazone, or dimethylsulfoxide vehicle for another 24 hr. Then, the cells were lysed and processed for luciferase assay. PPRE-directed luciferase expression was normalized with Renilla luciferase activity (internal control).

Analysis of Monoacylglycerol Species

Analysis of MAG species was as done previously (Zhao et al., 2014). Briefly, total lipids were extracted from visceral and brown fat from ABHD6 WT and KO mice. The extracted lipids were dissolved in 50 μl chloroform, and 1- and 2-MAGs were separated on thin layer chromatography plates.

Monoacylglycerol Hydrolysis Activity

Adipose tissues from HFD-fed ABHD6-KO and WT mice were quickly washed and homogenized in Krebs-Ringer bicarbonate hepes. Total MAG hydrolysis activity was measured in the tissue homogenates using 5 μM 1-S-arachidonoylthioglycerol and ThioGlo-1 (Covalent Associates) as fluorescent probe (Zhao et al., 2014).

Effect of PPARα and PPARγ Antagonists, In Vitro, on the Expression of Genes Related to Adipose Browning

Differentiated 3T3-L1 cells (Kohanski et al., 1986) and human primary adipocytes (Ahfeldt et al., 2012) and preadipocytes from ABHD6-KO and WT mice were prepared (Liu et al., 2010) as described before. The differentiated adipocytes were treated with 10 μM WWL70, 100 μM 1-oleoylglycerol in the absence or presence of 1 μM PPARα antagonist GW6471 (Wang et al., 2013), or 1 μM PPARγ antagonist T0070907 (Lee et al., 2002) for 24 hr, and then the cells were used for mRNA analysis of genes related to adipose browning.

Oxygen Consumption Rates in Adipocytes

Differentiated mouse 3T3-L1 cells and human adipocytes were treated overnight in DMEM medium with DMSO, 100 μM 1-oleoylglycerol, or 10 μM WWL70, without and with 1 μM GW6471. Next day, the incubation medium was replaced with unbuffered DMEM-based medium (Seahorse Bioscience) with 25 mM glucose with or without various inhibitors. Cells were incubated for 1 hr, and then the oxygen consumption rate was measured using XF analyzer (Seahorse Bioscience).

Statistical Analysis

Statistical analysis was performed using one-way ANOVA with Dunnett's post-test for multiple comparisons or two-way ANOVA with Bonferroni's post-test for multiple comparisons using GraphPad Prism. For browning gene expression results, comparisons were made by unpaired two-tailed Student's t test. Values are expressed as means ± SEM.

SUPPLEMENTAL INFORMATION

Supplemental Information includes Supplemental Experimental Procedures, seven figures, and one table and can be found with this article online at http://dx.doi.org/10.1016/j.celrep.2016.02.076.

AUTHOR CONTRIBUTIONS

S.Z. performed most of the experiments and helped design the study and participated in writing the manuscript. Y.M., C.A., and J.I. performed in vivo and ex vivo experiments. G.B. and J.M.B. designed and performed the WWL70 and ABHD6-ASO in vivo experiments. P.P., D.Z., T.A.N., and R.P. participated in genotyping and in vitro and respiration experiments. M.-L.P. and E.J. participated in the design of in vivo experiments and interpretation of the data. S.T. and S.F. designed and performed the behavior tests and interpreted the results. S.R.M.M. and M.P. designed and supervised the project, interpreted the data, and wrote the manuscript.

ACKNOWLEDGMENTS

This study was supported by funds from Canadian Institutes of Health Research grants to M.P. and S.R.M.M. and by a NIH grant (R01-HL122283) to J.M.B. and a CIHR grant and New Investigator award to S.F. M.P. holds the Canada Research Chair in Diabetes and Metabolism. Y.M. is supported by a fellowship from Fond de recherche Santé Québec (FRSQ). We thank the core facilities of Cellular Physiology & Metabolomics and Rodent Phenotyping of CRCHUM/Montreal Diabetes Research Center for the many metabolic analyses performed in this study. We also thank Dr. Julie Lavoie, Dr. Ines Holzbaur, and Dr. Kathryn Skorey for critically reading the manuscript.

Received: June 18, 2015
Revised: December 21, 2015
Accepted: February 18, 2016
Published: March 17, 2016

REFERENCES

Ahfeldt, T., Schinzel, R.T., Lee, Y.K., Hendrickson, D., Kaplan, A., Lum, D.H., Camahort, R., Xia, F., Shay, J., Rhee, E.P., et al. (2012). Programming human pluripotent stem cells into white and brown adipocytes. Nat. Cell Biol. *14*, 209–219.

Alhouayek, M., Masquelier, J., Cani, P.D., Lambert, D.M., and Muccioli, G.G. (2013). Implication of the anti-inflammatory bioactive lipid prostaglandin D2-glycerol ester in the control of macrophage activation and inflammation by ABHD6. Proc. Natl. Acad. Sci. USA *110*, 17558–17563.

Attané, C., Daviaud, D., Dray, C., Dusaulcy, R., Masseboeuf, M., Prévot, D., Carpéné, C., Castan-Laurell, I., and Valet, P. (2011). Apelin stimulates glucose uptake but not lipolysis in human adipose tissue ex vivo. J. Mol. Endocrinol. *46*, 21–28.

Attané, C., Foussal, C., Le Gonidec, S., Benani, A., Daviaud, D., Wanecq, E., Guzmán-Ruiz, R., Dray, C., Bezaire, V., Rancoule, C., et al. (2012). Apelin treatment increases complete fatty acid oxidation, mitochondrial oxidative capacity, and biogenesis in muscle of insulin-resistant mice. Diabetes *61*, 310–320.

Badin, P.M., Loubière, C., Coonen, M., Louche, K., Tavernier, G., Bourlier, V., Mairal, A., Rustan, A.C., Smith, S.R., Langin, D., and Moro, C. (2012). Regulation of skeletal muscle lipolysis and oxidative metabolism by the co-lipase CGI-58. J. Lipid Res. *53*, 839–848.

Bartelt, A., and Heeren, J. (2014). Adipose tissue browning and metabolic health. Nat. Rev. Endocrinol. *10*, 24–36.

Blankman, J.L., Simon, G.M., and Cravatt, B.F. (2007). A comprehensive profile of brain enzymes that hydrolyze the endocannabinoid 2-arachidonoylglycerol. Chem. Biol. *14*, 1347–1356.

Cereijo, R., Giralt, M., and Villarroya, F. (2015). Thermogenic brown and beige/brite adipogenesis in humans. Ann. Med. *47*, 169–177.

Di Marzo, V., and Matias, I. (2005). Endocannabinoid control of food intake and energy balance. Nat. Neurosci. *8*, 585–589.

Dirkx, E., van Eys, G.J., Schwenk, R.W., Steinbusch, L.K., Hoebers, N., Coumans, W.A., Peters, T., Janssen, B.J., Brans, B., Vogg, A.T., et al. (2014). Protein kinase-D1 overexpression prevents lipid-induced cardiac insulin resistance. J. Mol. Cell. Cardiol. *76*, 208–217.

Even, P.C., and Nadkarni, N.A. (2012). Indirect calorimetry in laboratory mice and rats: principles, practical considerations, interpretation and perspectives. Am. J. Physiol. Regul. Integr. Comp. Physiol. *303*, R459–R476.

Gnad, T., Scheibler, S., von Kügelgen, I., Scheele, C., Kilić, A., Glöde, A., Hoffmann, L.S., Reverte-Salisa, L., Horn, P., Mutlu, S., et al. (2014). Adenosine activates brown adipose tissue and recruits beige adipocytes via A2A receptors. Nature *516*, 395–399.

Haemmerle, G., Moustafa, T., Woelkart, G., Büttner, S., Schmidt, A., van de Weijer, T., Hesselink, M., Jaeger, D., Kienesberger, P.C., Zierler, K., et al.

(2011). ATGL-mediated fat catabolism regulates cardiac mitochondrial function via PPAR-α and PGC-1. Nat. Med. *17*, 1076–1085.

Hondares, E., Iglesias, R., Giralt, A., Gonzalez, F.J., Giralt, M., Mampel, T., and Villarroya, F. (2011a). Thermogenic activation induces FGF21 expression and release in brown adipose tissue. J. Biol. Chem. *286*, 12983–12990.

Hondares, E., Rosell, M., Díaz-Delfín, J., Olmos, Y., Monsalve, M., Iglesias, R., Villarroya, F., and Giralt, M. (2011b). Peroxisome proliferator-activated receptor α (PPARα) induces PPARγ coactivator 1α (PGC-1α) gene expression and contributes to thermogenic activation of brown fat: involvement of PRDM16. J. Biol. Chem. *286*, 43112–43122.

Kharitonenkov, A., and Adams, A.C. (2014). Inventing new medicines: The FGF21 story. Mol. Metab. *3*, 221–229.

Koh, H.J., Toyoda, T., Didesch, M.M., Lee, M.Y., Sleeman, M.W., Kulkarni, R.N., Musi, N., Hirshman, M.F., and Goodyear, L.J. (2013). Tribbles 3 mediates endoplasmic reticulum stress-induced insulin resistance in skeletal muscle. Nat. Commun. *4*, 1871.

Kohanski, R.A., Frost, S.C., and Lane, M.D. (1986). Insulin-dependent phosphorylation of the insulin receptor-protein kinase and activation of glucose transport in 3T3-L1 adipocytes. J. Biol. Chem. *261*, 12272–12281.

Lee, G., Elwood, F., McNally, J., Weiszmann, J., Lindstrom, M., Amaral, K., Nakamura, M., Miao, S., Cao, P., Learned, R.M., et al. (2002). T0070907, a selective ligand for peroxisome proliferator-activated receptor gamma, functions as an antagonist of biochemical and cellular activities. J. Biol. Chem. *277*, 19649–19657.

Liew, C.W., Bochenski, J., Kawamori, D., Hu, J., Leech, C.A., Wanic, K., Malecki, M., Warram, J.H., Qi, L., Krolewski, A.S., and Kulkarni, R.N. (2010). The pseudokinase tribbles homolog 3 interacts with ATF4 to negatively regulate insulin exocytosis in human and mouse beta cells. J. Clin. Invest. *120*, 2876–2888.

Liu, Q., Gauthier, M.S., Sun, L., Ruderman, N., and Lodish, H. (2010). Activation of AMP-activated protein kinase signaling pathway by adiponectin and insulin in mouse adipocytes: requirement of acyl-CoA synthetases FATP1 and Acsl1 and association with an elevation in AMP/ATP ratio. FASEB J. *24*, 4229–4239.

Liu, S., Xi, Y., Bettaieb, A., Matsuo, K., Matsuo, I., Kulkarni, R.N., and Haj, F.G. (2014). Disruption of protein-tyrosine phosphatase 1B expression in the pancreas affects β-cell function. Endocrinology *155*, 3329–3338.

Mauvais-Jarvis, F., Clegg, D.J., and Hevener, A.L. (2013). The role of estrogens in control of energy balance and glucose homeostasis. Endocr. Rev. *34*, 309–338.

Mottillo, E.P., Bloch, A.E., Leff, T., and Granneman, J.G. (2012). Lipolytic products activate peroxisome proliferator-activated receptor (PPAR) α and δ in brown adipocytes to match fatty acid oxidation with supply. J. Biol. Chem. *287*, 25038–25048.

Nadal-Casellas, A., Bauzá-Thorbrügge, M., Proenza, A.M., Gianotti, M., and Lladó, I. (2013). Sex-dependent differences in rat brown adipose tissue mitochondrial biogenesis and insulin signaling parameters in response to an obesogenic diet. Mol. Cell. Biochem. *373*, 125–135.

Nedergaard, J., and Cannon, B. (2014). The browning of white adipose tissue: some burning issues. Cell Metab. *20*, 396–407.

Nielsen, T.S., Jessen, N., Jørgensen, J.O., Møller, N., and Lund, S. (2014). Dissecting adipose tissue lipolysis: molecular regulation and implications for metabolic disease. J. Mol. Endocrinol. *52*, R199–R222.

Nookaew, I., Svensson, P.A., Jacobson, P., Jernås, M., Taube, M., Larsson, I., Andersson-Assarsson, J.C., Sjöström, L., Froguel, P., Walley, A., et al. (2013). Adipose tissue resting energy expenditure and expression of genes involved in mitochondrial function are higher in women than in men. J. Clin. Endocrinol. Metab. *98*, E370–E378.

Ohno, H., Shinoda, K., Spiegelman, B.M., and Kajimura, S. (2012). PPARγ agonists induce a white-to-brown fat conversion through stabilization of PRDM16 protein. Cell Metab. *15*, 395–404.

Owen, B.M., Ding, X., Morgan, D.A., Coate, K.C., Bookout, A.L., Rahmouni, K., Kliewer, S.A., and Mangelsdorf, D.J. (2014). FGF21 acts centrally to induce sympathetic nerve activity, energy expenditure, and weight loss. Cell Metab. *20*, 670–677.

Peyot, M.L., Pepin, E., Lamontagne, J., Latour, M.G., Zarrouki, B., Lussier, R., Pineda, M., Jetton, T.L., Madiraju, S.R., Joly, E., and Prentki, M. (2010). Beta-cell failure in diet-induced obese mice stratified according to body weight gain: secretory dysfunction and altered islet lipid metabolism without steatosis or reduced beta-cell mass. Diabetes *59*, 2178–2187.

Pfeifer, A., and Hoffmann, L.S. (2015). Brown, beige, and white: the new color code of fat and its pharmacological implications. Annu. Rev. Pharmacol. Toxicol. *55*, 207–227.

Prentki, M., and Madiraju, S.R. (2008). Glycerolipid metabolism and signaling in health and disease. Endocr. Rev. *29*, 647–676.

Richard, D., Carpentier, A.C., Doré, G., Ouellet, V., and Picard, F. (2010). Determinants of brown adipocyte development and thermogenesis. Int. J. Obes. *34* (*Suppl 2*), S59–S66.

Roberts, L.D., Boström, P., O'Sullivan, J.F., Schinzel, R.T., Lewis, G.D., Dejam, A., Lee, Y.K., Palma, M.J., Calhoun, S., Georgiadi, A., et al. (2014). β-Aminoisobutyric acid induces browning of white fat and hepatic β-oxidation and is inversely correlated with cardiometabolic risk factors. Cell Metab. *19*, 96–108.

Rosen, E.D., and Spiegelman, B.M. (2014). What we talk about when we talk about fat. Cell *156*, 20–44.

Shabalina, I.G., Petrovic, N., de Jong, J.M., Kalinovich, A.V., Cannon, B., and Nedergaard, J. (2013). UCP1 in brite/beige adipose tissue mitochondria is functionally thermogenic. Cell Rep. *5*, 1196–1203.

Sharma, S., and Fulton, S. (2013). Diet-induced obesity promotes depressive-like behaviour that is associated with neural adaptations in brain reward circuitry. Int. J. Obes. *37*, 382–389.

Spiegelman, B.M. (2013). Banting Lecture 2012: Regulation of adipogenesis: toward new therapeutics for metabolic disease. Diabetes *62*, 1774–1782.

Sumara, G., Formentini, I., Collins, S., Sumara, I., Windak, R., Bodenmiller, B., Ramracheya, R., Caille, D., Jiang, H., Platt, K.A., et al. (2009). Regulation of PKD by the MAPK p38delta in insulin secretion and glucose homeostasis. Cell *136*, 235–248.

Taschler, U., Radner, F.P., Heier, C., Schreiber, R., Schweiger, M., Schoiswohl, G., Preiss-Landl, K., Jaeger, D., Reiter, B., Koefeler, H.C., et al. (2011). Monoglyceride lipase deficiency in mice impairs lipolysis and attenuates diet-induced insulin resistance. J. Biol. Chem. *286*, 17467–17477.

Thomas, G., Betters, J.L., Lord, C.C., Brown, A.L., Marshall, S., Ferguson, D., Sawyer, J., Davis, M.A., Melchior, J.T., Blume, L.C., et al. (2013). The serine hydrolase ABHD6 Is a critical regulator of the metabolic syndrome. Cell Rep. *5*, 508–520.

Wang, W., Lin, Q., Lin, R., Zhang, J., Ren, F., Zhang, J., Ji, M., and Li, Y. (2013). PPARα agonist fenofibrate attenuates TNF-α-induced CD40 expression in 3T3-L1 adipocytes via the SIRT1-dependent signaling pathway. Exp. Cell Res. *319*, 1523–1533.

Wiernsperger, N.F. (2005a). Is non-insulin dependent glucose uptake a therapeutic alternative? Part 1: physiology, mechanisms and role of non insulin-dependent glucose uptake in type 2 diabetes. Diabetes Metab. *31*, 415–426.

Wiernsperger, N.F. (2005b). Is non-insulin dependent glucose uptake a therapeutic alternative? Part 2: Do such mechanisms fulfil the required combination of power and tolerability? Diabetes Metab. *31*, 521–525.

Wu, J., Boström, P., Sparks, L.M., Ye, L., Choi, J.H., Giang, A.H., Khandekar, M., Virtanen, K.A., Nuutila, P., Schaart, G., et al. (2012). Beige adipocytes are a distinct type of thermogenic fat cell in mouse and human. Cell *150*, 366–376.

Wu, J., Cohen, P., and Spiegelman, B.M. (2013). Adaptive thermogenesis in adipocytes: is beige the new brown? Genes Dev. *27*, 234–250.

Xue, B., Coulter, A., Rim, J.S., Koza, R.A., and Kozak, L.P. (2005). Transcriptional synergy and the regulation of Ucp1 during brown adipocyte induction in white fat depots. Mol. Cell. Biol. *25*, 8311–8322.

Zechner, R., Zimmermann, R., Eichmann, T.O., Kohlwein, S.D., Haemmerle, G., Lass, A., and Madeo, F. (2012). FAT SIGNALS–lipases and lipolysis in lipid metabolism and signaling. Cell Metab. *15*, 279–291.

Zhao, S., Mugabo, Y., Iglesias, J., Xie, L., Delghingaro-Augusto, V., Lussier, R., Peyot, M.L., Joly, E., Taïb, B., Davis, M.A., et al. (2014). α/β-Hydrolase domain-6-accessible monoacylglycerol controls glucose-stimulated insulin secretion. Cell Metab. *19*, 993–1007.

Zhao, S., Pourshariffi, P., Mugabo, Y., Levens, E.J., Vivot, K., Attane, C., Iglesias, J., Peyot, M.L., Joly, E., Madiraju, S.R., and Prentki, M. (2015). α/β-Hydrolase domain-6 and saturated long chain monoacylglycerol regulate insulin secretion promoted by both fuel and non-fuel stimuli. Mol. Metab. *4*, 940–950.

Zhu, L., Martinez, M.N., Emfinger, C.H., Palmisano, B.T., and Stafford, J.M. (2014). Estrogen signaling prevents diet-induced hepatic insulin resistance in male mice with obesity. Am. J. Physiol. Endocrinol. Metab. *306*, E1188–E1197.